

Article

Organic Geochemical Characteristics of the Upper Cretaceous Qingshankou Formation Oil Shales in the Fuyu Oilfield, Songliao Basin, China: Implications for Oil-Generation Potential and Depositional Environment

Wentong He ^{1,2,3} , Youhong Sun ^{1,2,4,*}, Wei Guo ^{1,2,*}, Xuanlong Shan ^{3,5}, Siyuan Su ^{5,6}, Shaopeng Zheng ^{1,2}, Sunhua Deng ^{1,2} , Shijie Kang ^{1,2} and Xu Zhang ^{1,2}

¹ College of Construction Engineering, Jilin University, Changchun 130021, China; Hewentong0510@163.com (W.H.); zhengsp0428@126.com (S.Z.); denghua13@163.com (S.D.); kangsj18@mails.jlu.edu.cn (S.K.); xuzhang18@mails.jlu.edu.cn (X.Z.)

² National-Local Joint Engineering Laboratory of In-situ Conversion, Drilling and Exploitation Technology for Oil Shale, Jilin University, Changchun 130021, China

³ Key Laboratory of Oil Shale and Coexistent Energy Minerals of Jilin Province, Changchun 130061, China; shanxl@jlu.edu.cn

⁴ School of Engineering and Techology, China University of Geosciences, Beijing 100083, China

⁵ College of Earth Sciences, Jilin University, Changchun 130000, China; susy@jlu.edu.cn

⁶ Shandong Provincial Key Laboratory of Depositional Mineralization & Sedimentary Mineral, Shandong University of Science and Technology, Qingdao 266590, China

* Correspondence: syh@jlu.edu.cn (Y.S.); guowei6981@jlu.edu.cn (W.G.)

Received: 8 October 2019; Accepted: 10 December 2019; Published: 14 December 2019



Abstract: The Cretaceous Era has always been a focus of geologic and palaeoenvironmental studies. Previous researchers believed that the impact of the global carbon cycle represents significant short-term global biogeochemical fluctuations, leading to the formation of a large number of organic rich sediments in the marine environment. During the Turonian, a large number of organic-rich oil shales were deposited in the lakes of the Songliao Basin in the Qingshankou Formation. How the depositional environment affected the formation of oil shales in continental lakes and the characteristics of these oil shales remain controversial. In this paper, through sampling of Qingshankou Formation strata, various testing methods are used to provide a variety of new data to study the characteristics of oil shales and palaeoenvironment evolution history in the Songliao Basin. The research of the sediments in the Qingshankou Formation in the Fuyu oilfield, Songliao Basin, via result analysis revealed that the oil shales possess an excellent oil-generation potential with moderate-high total organic carbon (TOC) levels (0.58–9.43%), high hydrogen index (HI) values (265–959 mg hydrocarbons (HC)/g TOC), high extractable organic matter (EOM) levels (2.50–6.96 mg/g TOC) and high hydrocarbon fractions (48–89%). The sources of the organic matter were mainly zooplankton, red algae and higher plants (including marine organisms). The aqueous palaeoenvironment of the Qingshankou Formation was a saline water environment with a high sulfate concentration, which promoted an increase in nutrients and stratification of the water density in the lake basin. Oxygen consumption in the bottom water layer promoted the accumulation and burial of high-abundance organic matter, thus forming the high-quality oil shales in the Qingshankou Formation. The global carbon cycle, warm-humid palaeoclimate, dynamic local biogeochemical cycling and relative passive tectonism were the most likely reasons for the TOC increase and negative $\delta^{13}\text{C}_{\text{org}}$ deviation.

Keywords: Qingshankou Formation; oil shale; Songliao Basin; oil-generation potential; depositional environment

1. Introduction

Cretaceous events have always been a focus of geological and palaeoenvironmental research, characterized by a greenhouse climate and repeated oceanic anoxic events (OAEs) [1]. OAEs occurred during the Aptian-Albian (OAE1), Cenomanian-Turonian (OAE2) and Coniacian-Santonian (OAE3). OAEs may be related to an increase in atmospheric greenhouse gas concentration [2], and the increase in atmospheric greenhouse gas concentration during OAEs may have been enhanced by rifting and volcanism [3]. Using the palaeo-barometer model, the CO₂ concentration from the Barremian to the Maastrichtian can be obtained using $\delta^{13}\text{C}$ of carbonates. The results show that there are two pCO₂ peaks in the whole Cretaceous period: the first peak occurs near the Cenomanian-Turonian (OAE2), and the second peak is at the S-C boundary. After the Early Campanian, the pCO₂ level decreased significantly [4,5], etc.

The impact of global carbon cycle is global in scale, which represents significant short-term global biogeochemical fluctuations, leading to large-scale formation of a large number of organic rich sediments in the marine environment [2]. The Songliao Basin is a large Cretaceous inland lake basin that has recorded abundant information on Cretaceous ancient lakes. The Qingshankou Formation is the main source rock in the Songliao Basin, and its formation period occurred after OAE2. There are many organic rich deposits in the Qingshankou Formation, which is also considered to be related to marine transgression [6].

Previous have found that Cretaceous marine black shales record stable isotope anomalies on a global scale. However, there is no definite conclusion on whether OAE2 is related to Cretaceous continental lakes, and a uniform explanation is lacking for the carbon isotope fluctuations in the Cretaceous Songliao Basin [1]. Song considered that the fluctuations in organic carbon isotopes in the Cretaceous strata were controlled by the input of terrestrial plants, while other report suggested that these fluctuations in organic carbon isotopes were related to the increase in dissolved CO₂ concentration in acidic and alkaline seawater and lake water [7]. Wan believed that the carbon isotope fluctuations of the Qingshankou Formation are a global-scale feature of Cretaceous strata, which may be related to OAE2 [8].

The interpretation of organic carbon isotopes is still very controversial. Organic carbon isotope and total organic carbon data alone are not enough to explain the changes in the carbon cycle; thus, other evidence is needed to substantiate these changes. Previous studies on the organic geochemistry of the Qingshankou Formation did not focus on the southeast uplift of the Songliao Basin, and the research objects were the mature mudstones of the Qingshankou Formation, not the oil shales. In this paper, an exploration well for the purpose of scientific research on the southeastern uplift of the Songliao Basin is established to obtain a complete stratum core of the Qingshankou Formation and to examine the geochemical characteristics at a high precision and study the characteristics of the oil shale resources, palaeoenvironment, evolution history and even the global climate change effects.

2. Geological Setting

2.1. Plate Tectonics and Stratigraphic Sequence in the Songliao Basin

The Songliao Basin is a large Cretaceous continental basins and the most typical intracratonic rift basin in Asia [9,10]. The Songliao Basin is a Cretaceous basin with a long history and a continuous sedimentation. Thick oil-bearing shales were deposited in the Qingshankou and Nenjiang Formations. The tectonic evolution of the Songliao Basin was controlled by mantle plume thermal energy and the eastern Pacific plate subduction. Mesozoic tectonic evolution can be divided into pre-rift, rift, post-rift thermal subsidence, compressional and weak extensional relaxation periods constituting five stages of evolution [11]. The total thickness of the sedimentary layer in the Songliao Basin is more than 5000 m, which is widely distributed. As a whole, the basin is a binary structure consisting of lower rift and upper depression basins, which has inherited typical tectonic and sedimentary characteristics of

continental rift basins. A very thick Mesozoic-Cenozoic layer has been deposited in Songliao Basin (Figure 1) [11,12].

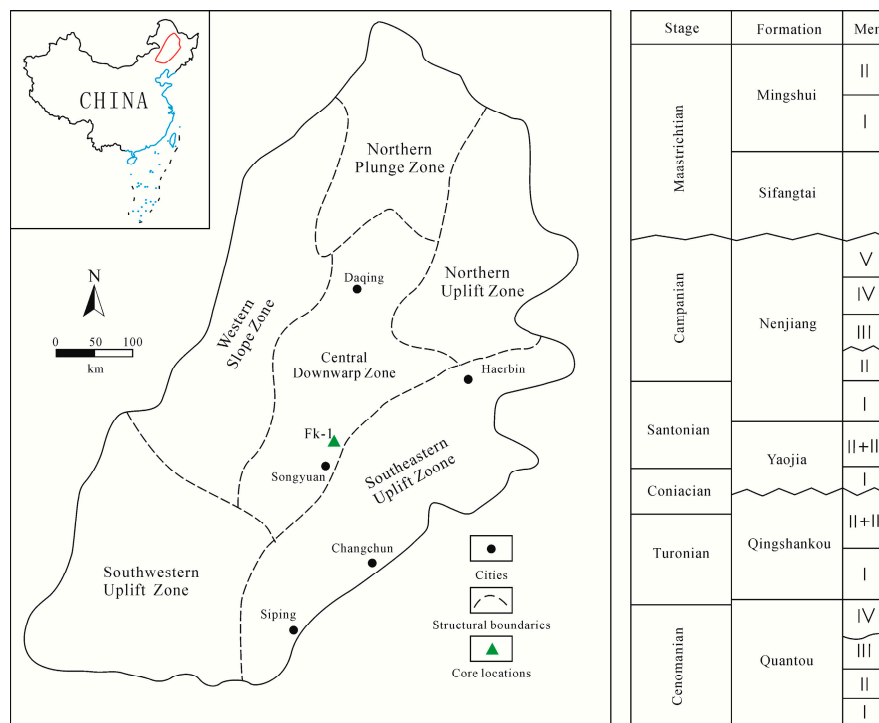


Figure 1. Geological map and stratigraphic histogram of Songliao Basin. The location of FK-1 well is indicated in the figure [11].

2.2. Qingshankou Formations

The Qingshankou Formation is divided into three parts. Zone1 of the Qingshankou Formation consists of dark grey mudstones and oil shales in the middle and eastern parts of the basin, while grey sandstones and siltstones are developed in the provenance areas in the west and north of the basin. A set of grey-green siltstone transgressive deposits are developed at the bottom of the Qingshankou Formation in most areas of the basin, which were identified via scientific research drilling (Figure 1) [13]. In parts 2–3 of the Qingshankou Formation, the grain size of the rocks gradually coarsened from bottom to top due to strengthening of the terrigenous supply and a decrease in the lake level, and the central depression developed into black mudstones with thin siltstones and Ostracoda bioclastic limestones. The Qingshankou Formation and lower Quantou Formation in the central depression exhibit integrated contacts, while unconformity contacts are mostly found in other areas [13,14].

At the bottom of the Qingshankou Formation, angiosperm pollens with important epochal significance have been observed, such as *Cranwellia*, *Lythraites*, and *Complexiopollis*. At the same time, *Borealipollis*, *Butinia*, *Areicipites*, and *Sabalpollenites* were found in the middle of the Qingshankou Formation. This shows that the Qingshankou Formation was deposited after the Turonian period of the Late Cretaceous [15,16]. The duration of the lake anoxic event occurring at the bottom of the zone1 of the Qingshankou Formation may be ~250 ka, which is similar to the duration of the OAE2 of the Cretaceous [17,18].

The study of Songhuajiang biota shows that the black shales at the bottom of the Qingshankou Formation may be equivalent to the black shales produced by anoxic events near the C-T boundary. The age of the oil-bearing shales at the bottom of the Qingshankou Formation may correspond to the Cenomanian-Turonian boundary [6,19–21].

Predecessors found three thin interbeds of tuff in dark mudstone of the lake facies of the Qingshankou Formation in the M-206 well. The U-Pb isotope ages of the volcanic limestone zircon in

these three layers are 91.4 ± 0.5 Ma, 90.1 ± 0.6 Ma and 90.4 ± 0.4 Ma in zone2. This U-Pb isotopic dating indicates that the bottom boundary of the Qingshankou Formation was the Turonian stage rather than the Cenomanian stage [15,22,23]. With the completion of the Continental Scientific Drilling Project of the creative Songliao Basin (SK-1), more scientific evidence has been provided [24–26]. The latest chronostratigraphic and geochemical data show that the Qingshankou Formation is 92–86 Ma old, and the top of the underlying Quantou Formation is from the Cenomanian-Turonian [12]. The ancient lake anoxic event (LAE1) corresponding to the lower zone of the Qingshankou Formation lasted for approximately 250 ka, which is similar to the duration of Cretaceous C-T OAE2 that occurred at least 2 million years before LAE1 (93.9 Ma) [18,24,27].

3. Materials and Methods

The FK-1 drilling programme was implemented 26 km north-east of Songyuan city, and the complete Qingshankou Formations cores were obtained (Figure 1). The FK-1 drilling programme recovered 455 m of continuous cores at a recovery ratio of 96.8%. According to the core cataloguing results, Quaternary sandy soil occurs from 45 m (meters) below the surface to the underground, and no core has been collected. All cores, 137 samples, were cleaned with distilled water, and the cores were dried at 80°C for 12 h and then crushed to 200 mesh with a ceramic ring mill. The 137 samples were tested for total sulfur (TS), TOC, organic carbon isotope and pyrite sulfur isotope (Figure 2). Based on the results, 10 samples were selected for biomarker analysis and compound-specific carbon isotope analysis, and 20 samples were selected for organic petrographic analysis.

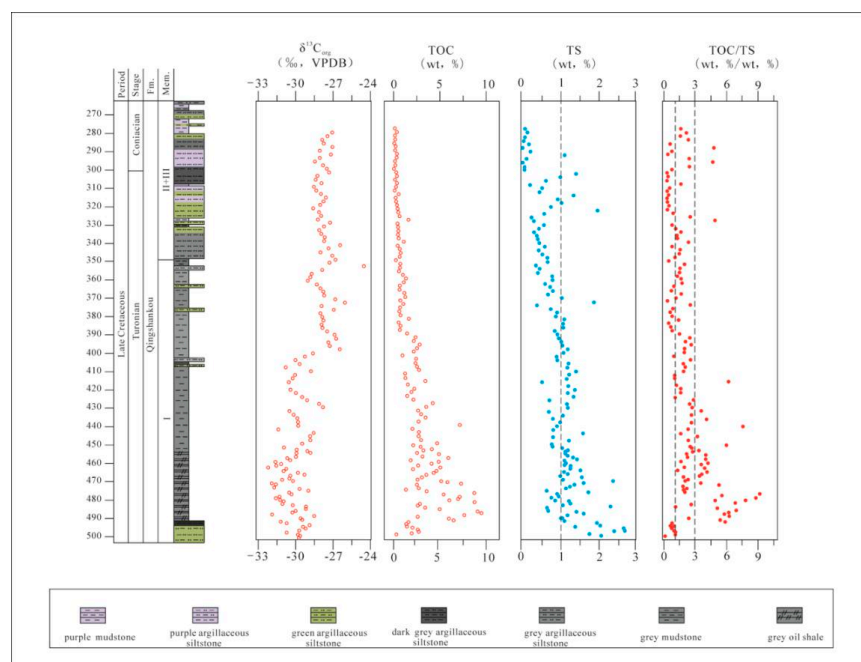


Figure 2. Chemostratigraphy of FK-1 well core samples from the Qingshankou formations.

Analysis of the rock pyrolysis TS, TOC, organic carbon isotopes and determination of specific compounds and biomarkers were conducted at the Key Laboratory of Oil Shale and Coexistent Energy Minerals of Jilin Province. A Rock Eval-6 analyser (Institut Francais Du Petrole) was used in the rock pyrolysis experiments. The critical parameters of S1, S2, and S3 were measured, whereas the hydrogen index (HI) and oxygen index (OI) were calculated accordingly.

The sulfur abundance was determined by a PYRO cube elemental analyser (Elementar Analysensysteme GmbH) via combustion into SO_2 (assuming that the elemental S can be neglected in these samples). Two barium sulfate standards (IAEA-SO-5, barium sulfate) were added to each group of 10 samples. The error between the test values at each analysis stage was less than 0.5‰.

The TS content was also obtained. The determination method of the organic carbon abundance and organic carbon isotope composition is similar to that of the sulfur isotopes. Two standard samples, (GBW04408, caffeine), were added to each group of 10 samples, and the error between the standard samples was 0.5‰.

Carbon isotope determination of specific compounds in the saturated hydrocarbon component of the samples were performed using an Agilent 7890B gas chromatograph attached and an ISOprime100 isotope ratio mass spectrometer (ISOprime, Elementar Analysensysteme GmbH). Carbon dioxide was injected at the beginning and end of analysis and the GC column and temperature program had the same analytical error as the gas chromatography–mass spectrometry procedure of less than 0.5%.

4. Results and Discussion

4.1. Petrography

A core was collected in well FK-1 in the Qingshankou Formation at 280–496 m, and the Qingshankou Formation is mainly a set of dark sandstone-mudstone sedimentary assemblages. Through core observation, it is found that the Qingshankou Formation is dominated by deep and semi-deep lake facies mudstones, with some calcareous siltstone and bioclastic limestone beds. The core of the Qingshankou Formation is severely fractured, and the fragmentation pattern has a certain regularity. There are three main kinds of wedges: thin sheets (approximately 1 cm thick) and thick sheets (over 3 cm thick), and the shallower the burial depth is, the lower the proportion of thin cores is. Because the core mainly consists of mudstone, the sedimentary structure in the Qingshankou Formation is mainly a bedding structure, with mostly massive, horizontal and ripple bedding. The fossils, such as Phyllostachys, Ostracoda and plant debris, are locally enriched and stratified. Many characteristics are different from those of parts 2–3, reflecting different information of ancient lake water bodies. The color of the mudstone in zone1 is basically grey-black, which is notably deeper than those of the mudstones in parts 2–3. The bedding structure in zone1 is mainly horizontal bedding. A large number of ostracods and phyllodes can be found in parts 2–3, but hardly any occur in zone1. The frequency of limestone-mudstone and calcite beds in zone1 is significantly higher than that in parts 2–3. This shows that the water depth during deposition of zone1 increased and that the bottom water body was more anoxic during the sedimentary period.

4.2. Bulk Geochemical Parameters

4.2.1. TOC, TIC, TS and Pyrolysis

Zone1 of the Qingshankou Formation, located at the C-T boundary, is the main developed oil shale stratum. The TOC ranges from 0.58 to 9.43 wt% with an average of 3.44 wt%, and the TIC ranges from 0.003 to 0.46 wt% with an average of 0.09 wt% (thin carbonate beds excluded), while the TS content ranges from 0.55 to 2.41 wt% with an average of 1.17 wt% (Table 1).

Through the comparison of the latest core data of SK-1 well, it is found that there is a high TOC value (2–8%) in zone1 [27,28], which is consistent with the fluctuation trend of this research data. It can be seen that regional geochemical events occurred in this period.

A total of 20 oil shale samples were selected for rock pyrolysis experiments. The results showed that the TOC contents and pyrolysis S₂ values were generally elevated. According to Peters [29] these samples have very good to excellent hydrocarbon generating potential. (Table 1; Figures 2 and 3). Additionally, the samples had high or moderate hydrogen index (HI) and low Oxygen Index (OI) values in the range of 265–959 mg HC/g TOC and 0.41–8.44 mg CO₂/g TOC, respectively (Table 1). The T_{max} of the analysed oil shale samples, representing the temperature at which S₂ is at its maximum, is in the range of 419–430 °C. Generally, T_{max} reflects the thermal maturity, but it may also be affected by the type of kerogen [29,30]. Guo tested the vitrinite reflectance of the Qingshankou Formation oil

shales in the southeast uplift region of the Songliao Basin in 2012. The results show that the Ro value is between 0.47% and 0.63%, which also shows that the organic matter of the Qingshankou Formation in the Songliao Basin is mainly in the low-mature stage. Comparison of HI and T_{max} data showed that most of the samples were located in the immature zone of type I and type II kerogen (Figure 4).

Table 1. Results of pyrolysis, TOC, TIC, and TS analyses with calculated parameters and measured.

Sample ID	Deep (m)	TIC (wt%)	TOC (wt%)	TS (wt%)	TOC/TS	S1 (mg/g)	S2 (mg/g)	T_{max} (°C)	S3 (mg/g)	S1+S2 (mg/g)	HI	OI	PI
FKP-1	438	0.11	2.72	1.01	2.69	0.16	15.39	419	0.23	15.55	564.82	8.44	0.01
FKP-2	440	0.13	7.14	0.94	7.58	0.16	15.39	420	0.21	15.55	215.47	2.94	0.01
FKP-3	444	0.06	2.75	1.62	1.70	0.16	15.51	420	0.2	15.67	563.15	7.26	0.01
FKP-4	448	0.03	2.94	1.25	2.35	0.15	15.47	420	0.19	15.62	525.37	6.45	0.01
FKP-5	450	0.00	4.67	0.78	5.96	0.26	27.24	422	0.16	27.5	583.50	3.43	0.01
FKP-6	452	0.05	2.92	1.08	2.70	0.26	27.25	420	0.16	27.51	931.74	5.47	0.01
FKP-7	454	0.01	3.21	1.16	2.77	0.17	26.35	427	0.16	26.52	820.65	4.98	0.01
FKP-8	456	0.05	4.88	1.22	3.99	0.16	26.55	427	0.17	26.71	544.02	3.48	0.01
FKP-9	458	0.06	5.87	1.45	4.04	0.13	23.56	427	0.11	23.69	401.36	1.87	0.01
FKP-10	462	0.03	2.59	1.30	1.99	0.14	24.02	427	0.13	24.16	928.38	5.02	0.01
FKP-11	464	0.02	4.09	1.55	2.64	0.27	34.08	428	0.12	34.35	833.62	2.94	0.01
FKP-12	468	0.01	4.03	1.60	2.53	0.28	35.64	430	0.11	35.92	883.68	2.73	0.01
FKP-13	472	0.03	7.35	1.39	5.28	0.27	40.44	430	0.09	40.71	549.88	1.22	0.01
FKP-14	476	0.01	3.61	1.77	2.04	0.27	30.96	430	0.09	31.23	856.86	2.49	0.01
FKP-15	478	0.04	5.42	0.97	5.60	0.18	17.8	427	0.04	17.98	328.21	0.74	0.01
FKP-16	480	0.18	6.96	0.89	7.87	0.18	18.47	428	0.03	18.65	265.25	0.43	0.01
FKP-17	484	0.17	2.57	2.34	1.10	0.33	24.7	427	0.02	25.03	959.26	0.78	0.01
FKP-18	486	0.02	4.92	0.71	6.92	0.32	24.17	428	0.02	24.49	491.03	0.41	0.01
FKP-19	490	0.01	3.50	1.05	3.35	0.35	29.7	427	0.04	30.05	848.91	1.14	0.01
FKP-20	492	0.04	6.42	1.10	5.84	0.37	27.15	426	0.03	27.52	422.73	0.47	0.01

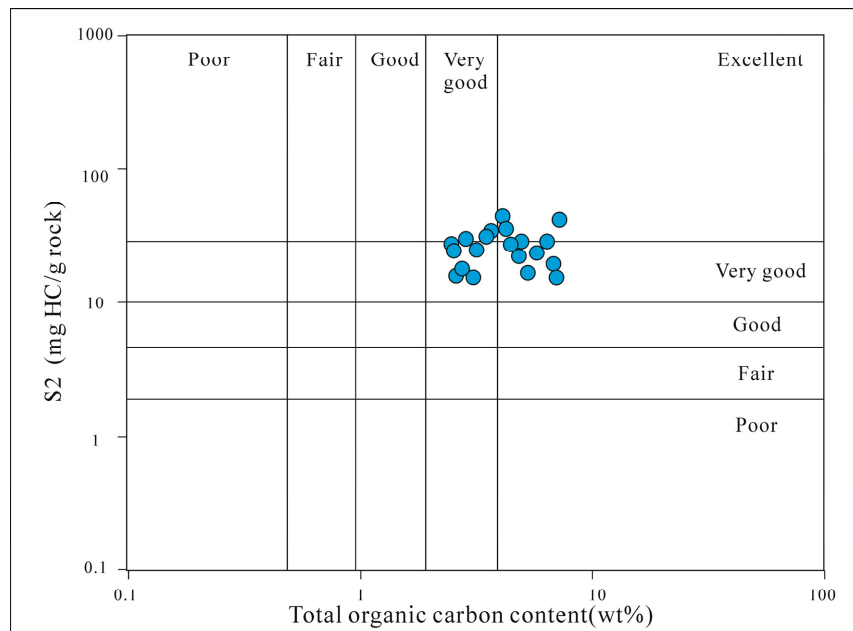


Figure 3. Plot of pyrolysis S2 versus total organic carbon (TOC) of the samples of the Qingshankou Formation [29].

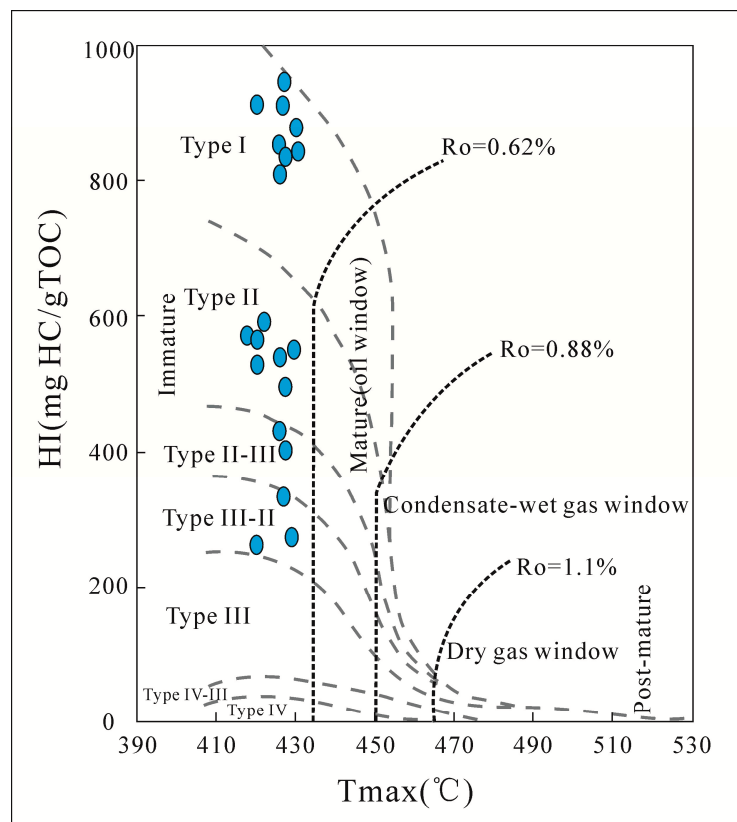
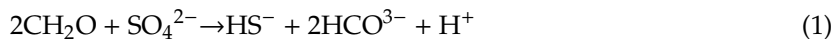


Figure 4. Plot of HI versus T_{max} of the analyzed samples of the Qingshankou Formation.

4.2.2. TOC/TS Ratio

In the process of enrichment and burial of the organic matter in sediments, hydrogen sulfide is formed by reaction of organic matter and sulfate in lakes under the action of reducing bacteria. The formed H_2S reacts with iron ions or oxides to form pyrite, which is called microbial sulfate reduction (MSR). Previous studies have shown that under experimental conditions, the MSR reaction affects most of the burial process and lead to pyritization of organic matter [31].

The MSR reaction is as follows:



It can be seen from the above reaction formulas that FeS_2 is mainly controlled by the sulfate, organic matter abundance and dissolved iron concentration in water and sedimentary environments. The most favorable formation environment of oil shale is an anaerobic environment with high concentrations of organic carbon and sulfate. Previous studies have shown that sulfate reduction usually occurs at sediment and water interfaces in oxidizing seabed environments. When a sulfidic and stratified water medium is used, pyrite can form at the sediment-water interface, resulting in a significant decrease in the TOC/TS ratio. When the ratio is lower than 1, the sulfates dissolved in pore water or deep water forms a sulfidic environment [32–38]. In continental lakes, the dissolved iron supply and organic matter productivity are higher than those in marine environments [39]. The sulfate content is the greatest factor restricting the formation of pyrite, and the sediment exhibits a higher TOC/TS ratio. Therefore, previous researchers used the TOC/TS ratio as a reference for distinguishing seawater and non-seawater environments [33,34]. In modern normal marine sediments, the TOC/TS ratio is 2.8 ± 0.8 approximately. The TOC/TS ratio of freshwater is often much higher [34].

At the top section of the Quantou Formation and in the bottom of the Qingshankou Formation, the test results show the high TOC, the high TS and the very low TOC/TS values (most of the ratios are less than 1), which indicates that the pore or deep water may be influenced by the sea. Extensive sulfidic environments entering the translucent zone can provide the required electrons for anaerobic photosynthetic autotrophy, and other sulfide-oxidizing bacteria will survive along the interface of the climacteric layer in the basin [40,41]. The average sulfur content in the bottom of the zone 1 (493–390 m) is 0.9%, which is higher than that in the overlying sediments, indicating that the sulfate concentration has reached a high level. A higher concentration of sulfate is characteristic of a high-salinity water environment [34]. Thus the Songliao Basin in this stage was represented by a brackish water-saline water environment, as was suggested earlier [15,23]. The TOC/TS ratio in the top section of the Qingshankou Formation at 390–352 m returned to a low value again, possibly due to oxidation of the organic matter [41,42]. The sediments of the zones 2–3 of the Qingshankou Formation are coarse silty mudstones and sandstones. TOC and TS are relatively low, and the TOC/TS ratio varies greatly, which may be due to distinct provenance changes of the zones 2–3, thus weakening the significance of the indicated sedimentary environment (Figure 2) [11].

4.3. Organic Geochemistry

4.3.1. Compositions of the Extracted Oil

Table 2 shows the extractable organic matter (EOM, 2.50–6.96 mg/g, TOC) of oil shale samples and the relative ratios of saturated hydrocarbons, aromatic hydrocarbons, NSO compounds and asphaltene. Higher relative proportions of hydrocarbons are obtained from the oil shale samples (48–89%) (Figure 5; Table 2).

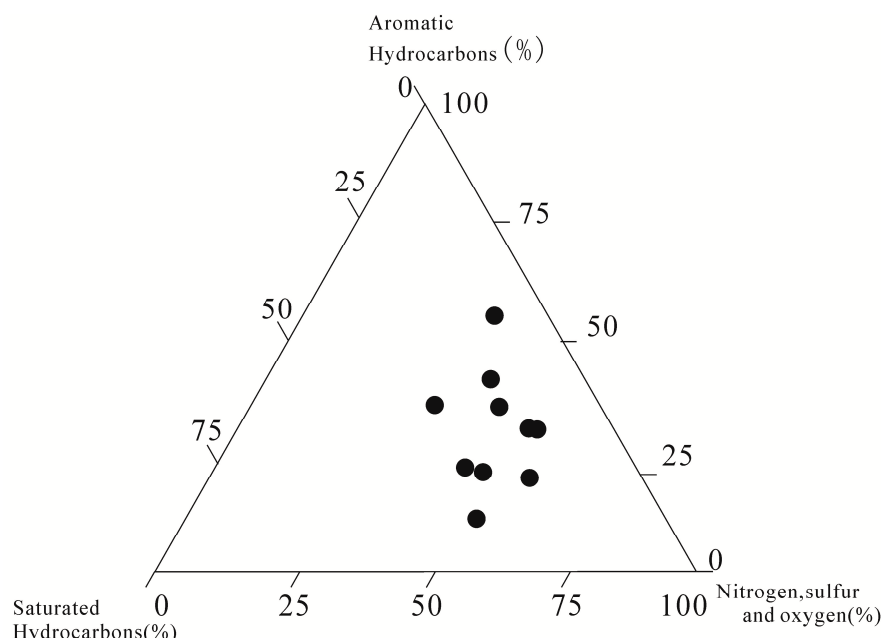


Figure 5. Ternary diagram of the extracted oil shale samples [43].

Table 2. Bulk geochemical results of the analyzed oil samples.

Sample ID	Depth (m)	Lithology	Extractable Organic Matter (mg/g TOC)	Chromatographic Fractions of Bitumen Extraction (Oil wt. %)					CPI	Normal Alkanes and Isoprenoids			Regular Steranes (<i>m/z</i> 217)				C27/C29
				Saturated Hydrocarbons	Aromatic Hydrocarbons	NSO Compounds	HCs	Sat/Aro%		Pr/Ph	Pr/nC17	Ph/nC18	Gl _a	$\alpha\alpha\alpha C_{27}\text{steranes}/m(\alpha\alpha\alpha C_{27}-C_{28}-C_{29}\text{steranes})$	$\alpha\alpha\alpha C_{28}\text{steranes}/m(\alpha\alpha\alpha C_{27}-C_{28}-C_{29}\text{steranes})$	$\alpha\alpha\alpha C_{29}\text{steranes}/m(\alpha\alpha\alpha C_{27}-C_{28}-C_{29}\text{steranes})$	
FKO-1	438.00	Oil shale	3.5	0.36	0.12	0.52	0.48	2.94	1.22	0.84	1.16	1.58	0.34	0.43	0.15	0.42	1.04
FKO-2	444.00	Oil shale	2.75	0.59	0.23	0.17	0.83	2.55	1.1	0.58	1.26	1.78	0.28	0.42	0.16	0.42	1
FKO-3	450.00	Oil shale	4.67	0.33	0.31	0.36	0.64	1.04	1.39	0.91	1.24	1.48	0.15	0.67	0.15	0.18	3.66
FKO-4	454.00	Oil shale	5.87	0.4	0.2	0.4	0.6	1.94	1.32	0.67	1.3	1.88	0.23	0.56	0.16	0.28	1.99
FKO-5	458.00	Oil shale	4.37	0.5	0.28	0.23	0.77	1.78	1.25	0.54	1.28	1.75	0.37	0.48	0.13	0.39	1.22
FKO-6	466.00	Oil shale	5.14	0.56	0.16	0.28	0.72	3.54	1.4	0.82	1.36	1.11	0.19	0.41	0.23	0.36	1.13
FKO-7	472.00	Oil shale	4.61	0.47	0.31	0.23	0.77	1.51	1.02	0.52	0.76	1.19	0.44	0.58	0.15	0.29	2.03
FKO-8	478.00	Oil shale	6.96	0.44	0.21	0.35	0.65	2.16	1.23	1.18	0.82	1.33	0.15	0.59	0.14	0.28	2.13
FKO-9	484.00	Oil shale	4.37	0.54	0.16	0.3	0.7	3.38	1.1	0.9	0.92	1.34	0.18	0.52	0.16	0.32	1.63
FKO-10	490.00	Oil shale	2.5	0.55	0.33	0.11	0.89	1.65	1.22	0.73	1.05	1.04	0.31	0.46	0.19	0.36	1.26
Minimum			2.5	0.33	0.12	0.11	0.48	1.04	1.02	0.52	0.76	1.04	0.15	0.41	0.13	0.18	1
Maximum			6.96	0.56	0.31	0.4	0.89	3.54	1.4	1.189	1.37	1.88	0.84	0.67	0.24	0.42	3.66
Average			4.47	0.47	0.23	0.29	0.71	2.25	1.23	0.77	1.12	1.45	0.31	0.51	0.16	0.33	1.72

CPI: carbon preference index; GI (Gammacerane Index): gammacerane/C₃₀ hopane.

4.3.2. Molecular Composition of Hydrocarbons

The *n*-alkanes are mainly composed of short-chain *n*-alkanes whose size ranges from *n*-C₁₉ to *n*-C₂₃, which is consistent with the main input characteristics of algae and bacteria (Figure 6 and Table 2) [44]. The acyclic isoprenoids pristane (Pr) and phytane (Ph) were found in all samples. In the field of sedimentary environment research, the ratio of pristane (Pr) to phytane (Ph) is a common index of redox conditions. The distributions of the Pr/Ph ratio in the samples ranged from 1.0 to 3.0, indicating sub-oxic depositional conditions, while the Pr/Ph ratios above 3.0 and below 0.6 indicated oxidizing and anoxic conditions, respectively [45].

In this study, it was found that the Pr/Ph ratio ranged from 0.52 to 1.18, which further indicates an anoxic formation environment. There are also studies showing that the Pr/Ph ratio is also affected by maturity. (Table 2) [46–48]. Because of the low maturity of all the oil shale samples studied, the influence of maturity can be excluded. In addition, the relationship between the ratio of Pr/*n*-C₁₇ and Ph/*n*-C₁₈ has been widely used in the classification and correlation of oil source rocks and the study of oil-generating environments [49,50]. Pr/*n*-C₁₇ and Ph/*n*-C₁₈ diagrams further demonstrate the algal/microbial source of the organic matter deposited in a reducing environment [51] (Figure 7; Table 2).

The m/z 217 mass chromatograms of the saturated hydrocarbons in analytical samples show terpane and steroid distributions, including conventional steroids C₂₇, C₂₈ and C₂₉ related to parent material sources (Figure 6). The distribution of steroids obtained by mass spectrometry showed similar characteristics for all samples.

In 1979, Huang and Menschein proposed the use of the relative proportions of the C₂₇, C₂₈ and C₂₉ steroids to determine the input of the source oil in a given environment. The relative proportions of the C₂₇ steranes are the highest (41~67%), followed by the C₂₈ (13~24%) and C₂₉ steranes (18~42%) (Table 2; Figure 8). C₂₈ sterols are often regarded as biomarkers of diatom, green algae and higher plants. [43], whereas C₂₇ steroids representing marine sediments are typical zooplankton and red algae and C₂₉ steroids are found in higher plants and some brown algae or green algae. [52] According to the ratios of the relative contents of the C₂₇, C₂₈ and C₂₉ steroids, it can be concluded that the oil shales are dominated by zooplankton, algae and higher plants. The relative content of the C₂₇ steroids exceeded that of the C₂₉ steroids, which may indicate a marine origin of the organic matter.

Previous studies have shown that a large amount of gammacerane usually occurs in organic matter deposits in high-salinity environments, and the presence of gammacerane can also indicate high-salinity environments [53]. It was observed that the gammacerane index (GI = gammacerane/αβC₃₀ hopane) decreased upwards. Therefore, the small fluctuations in Pr/Ph indicate the evolution from an anoxic saline water environment to an anoxic brackish water environment (Figure 9 and Table 2) [54]. There is a positive correlation between the sulfur content and GI in most samples. Samples with a high sulfur content and low TOC/TS ratio are characterized by high GI values, indicating an increased salinity in the water column and associated sulfate concentrations. This may reflect the formation environment of the oil shales, the large area of the lake basin, and the short-term seawater intrusion leading to water stratification, thereby forming a closed anoxic environment with a high salinity in the bottom layer, which enriched the organic matter with gamma paraffin. In the later period, the seawater channel entering the lake basin closed, and the salinity of the closed anoxic environment of the lake bottom slowly decreased to the normal value under the closed anoxic environment [21].

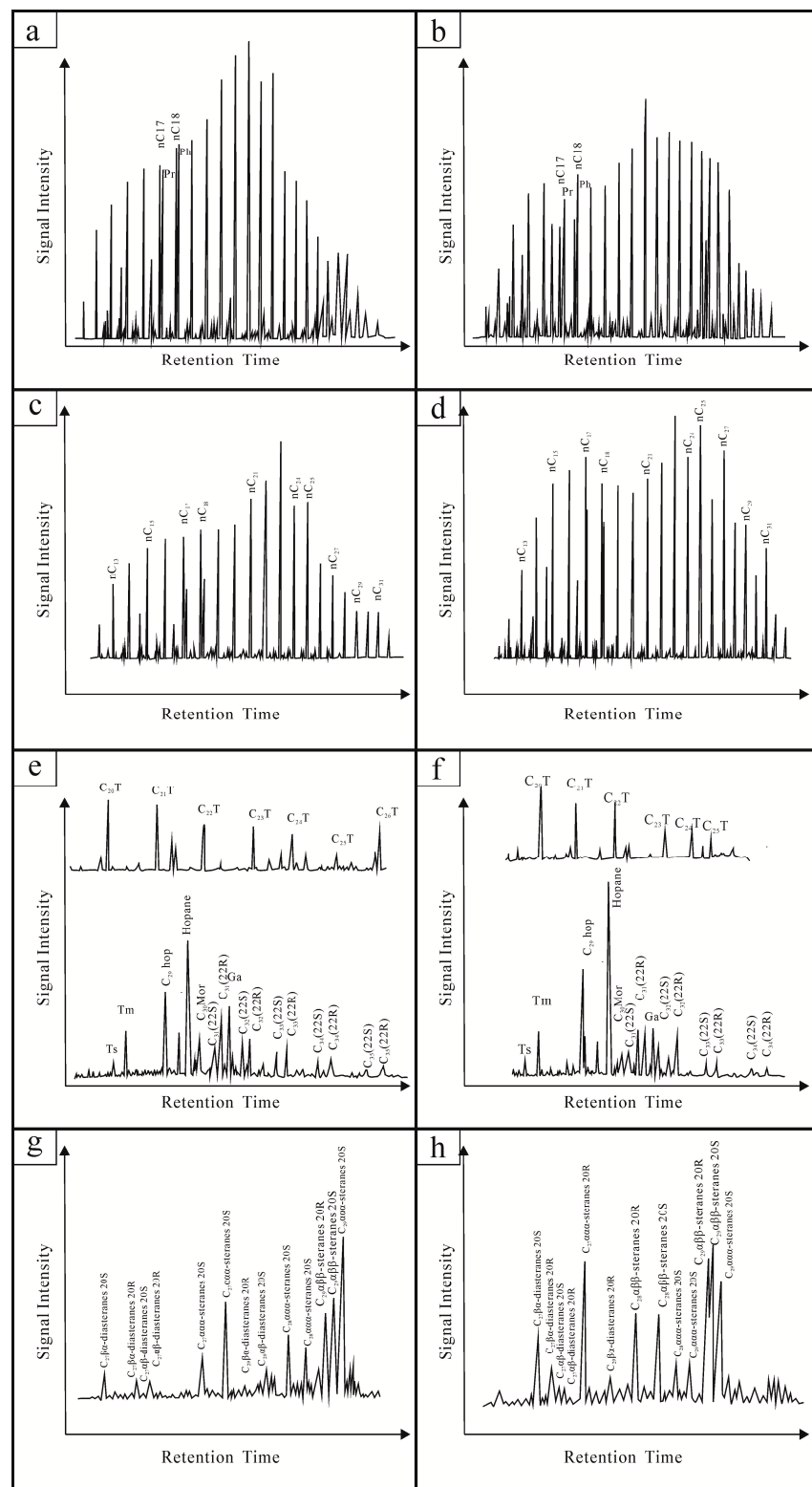


Figure 6. (a,b): Total inorganic carbon mass chromatograms (TIC), (c,d): m/z 85 ion chromatograms of the saturated hydrocarbons, (e,f): m/z 191 ion chromatograms of the saturated hydrocarbons and (g,h): m/z 217 ion chromatograms of the saturated hydrocarbons of the extracted oil from oil shale of the first zone of Qingshankou Formation.

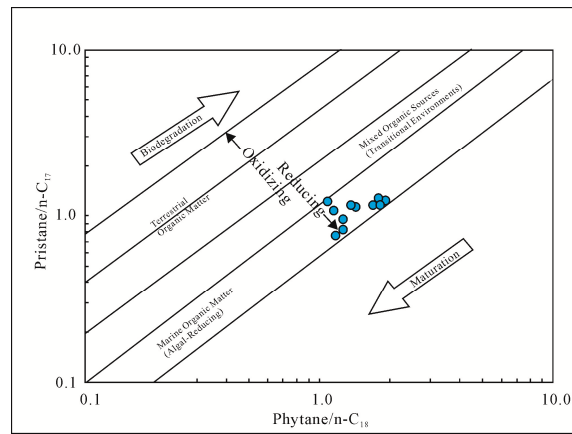


Figure 7. The relationship between pristane/ $n\text{-C}_{17}$ versus phytane/ $n\text{-C}_{18}$ [51].

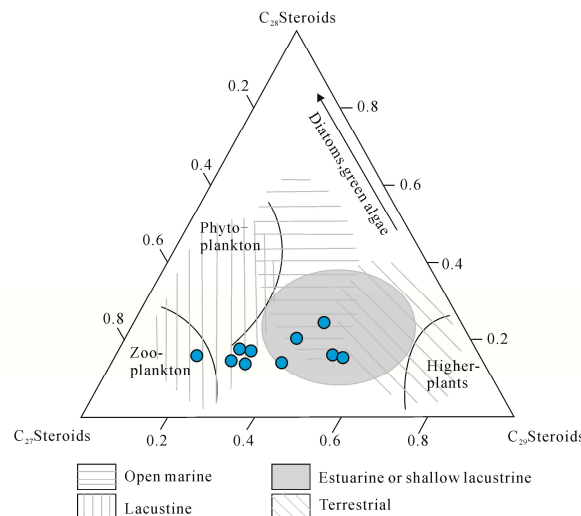


Figure 8. Ternary plot of relative proportions of C_{27} , C_{28} , and C_{29} steranes for the Qingshankouzu Formation, indicating the relationships between these sterane compositions [42,43].

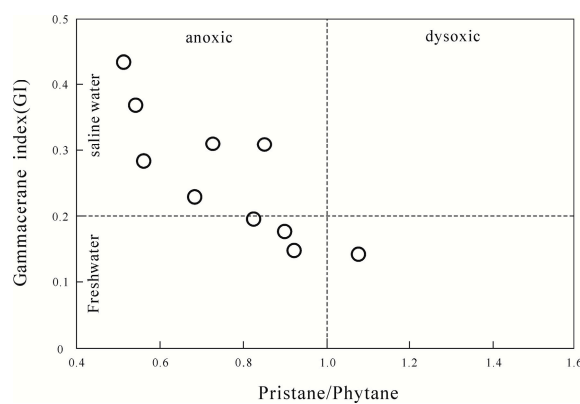


Figure 9. The relationship between gammacerane index and Pr/Ph [21,54].

4.3.3. Carbon Isotope Characteristics of the Monomer Hydrocarbons.

The carbon isotopic composition of the n -alkanes and pristane and phytane samples from the Qingshankou Formation is shown in Figure 10.

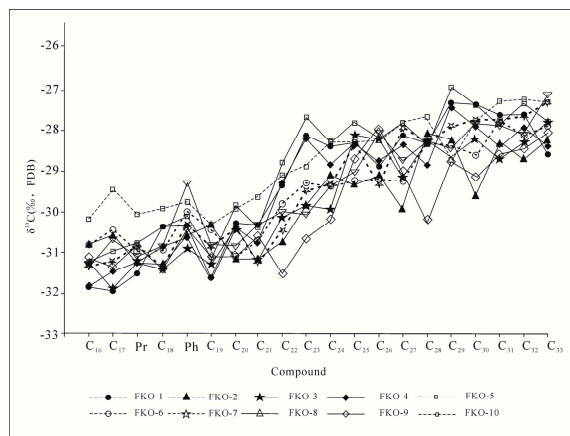


Figure 10. Carbon isotopic composition of *n*-alkanes, pristane and phytane in the saturated hydrocarbon fractions of selected samples from the Qingshankou Formation.

The carbon isotope composition of monomer hydrocarbons can provide genetic information of the organic matter in sediments. Carbon isotope analysis of the monomer hydrocarbons of the oil shales in the zone 1 shows that the carbon isotopes of the oil shale monomers in the zone 1 are relatively light and distributed between -30.7‰ and -26.4‰ , reflecting the contribution of lacustrine organic matter. It is generally believed that terrestrial organic matter is a mixture of sapropelic and humic components to varying degrees. The carbon isotope distribution curve of *n*-alkanes in lacustrine organic matter generally increases with increasing carbon number [55,56], and the carbon isotope distribution of the *n*-alkanes in the zone 1 shows no clear change from *n*-C₁₆ to *n*-C₂₃, which gradually becomes heavier after *n*-C₂₃, reflecting that the sources of the high-carbon and low-carbon organic matter are similar, mainly the input of lacustrine organic matter, and higher plant input accounts for a small proportion.

4.4. Changes in the Total Organic Carbon Isotopes

The $\delta^{13}\text{C}_{\text{org}}$ data show that the organic carbon isotope level is low from the bottom to the middle of zone 1 (495–395 m) and gradually changes from approximately -33‰ to -29‰ . Moreover, the TOC content of this section is high, averaging 3.8%. The $\delta^{13}\text{C}_{\text{org}}$ data of the upper part of zone 1 and zones 2–3 (395–280 m) show a significant positive deviation between -29 and -26‰ , and the TOC content decreases at the same time, averaging only 0.66% (Figure 4). Previous researchers also obtained $\delta^{13}\text{C}_{\text{org}}$ data by testing the continental scientific drilling (SK-1) core, and the overall trend was consistent with this study [27,28]. The records show that the negative $\delta^{13}\text{C}_{\text{org}}$ and positive TOC of Qingshankou formation indicate a “sharp” event, rather than a gradual evolution of the whole Turonian period.

Cretaceous events have always been a focus of geological and palaeoenvironmental studies, characterized by a greenhouse climate and repeated OAEs [1]. OAE2 occurs near the Cenomanian-Turonian boundary (93.9 Ma) [28,37], OAE2 has a duration of 400–850 ka, and the impact of OAE2 is global. [2,3,57,58] OAE2 is believed to be associated with activities in the submarine volcanic province and may begin with an increase in the rate of seafloor expansion. Submarine volcanoes and hydrothermal activities released a large amount of greenhouse gases including CO₂ into atmosphere and supplied many nutrients to the ocean, which significantly stimulated bioproductivity [5,24,59]. Moreover, other studies have shown that long-term changes in the CO₂ concentration during the Cretaceous are closely related to palaeotemperature changes [60–62]. Geochemical evidence also confirms the increase in continental weathering rate with increasing temperature during Turonian. The increases in continental weathering rate and hydrological cycle increased the input flux of nutrients to the ocean and promoted the increase in organic matter production. The increase in freshwater input may also have aggravated the stratification of oceans and seaways [63–65].

With the increase in atmospheric CO₂ concentration, the original balance of ¹³C and ¹²C between CaCO₃ and CH₂O is disrupted, and the fractionation value of carbon isotopes will increase

significantly [41]. The increase in atmospheric CO₂ concentration will directly lead to an increase in the dissolved CO₂ content in the lake basin, resulting in significant depletion of δ¹³C_{org} in photosynthetic products. Therefore, the increase of dissolved CO₂ is probably the one reason for the increase in TOC content and the negative δ¹³C_{org} deviation near the Cenomanian-Turonian boundary.

The typical greenhouse conditions during the Turonian period resulted in a warm and humid palaeoclimate. Cretaceous climate fluctuations in the Bering Strait region by means of δ¹⁸O values and flora distributions, suggest that the climate was warmer. Water regulation and gas exchange constraints of leaf stomata are the main controlling factors of carbon isotopes [66]. When climate conditions are wet, terrestrial plants can open their stomata or increase the number of stomata in lower leaves to absorb water, and the water use efficiency will increase significantly and carbon isotope fractionation in plants will increase and lead to more negative δ¹³C values in leaves. This is consistent with the palaeoclimatic conditions studied by Yan Jingjing et al. [67] through sporopollen studies. There was a higher humidity near the boundary period of the zone1, and then the climate gradually became dry. Therefore, the warm and humid palaeoclimate may be another reason behind the negative δ¹³C_{org} deviation near the C-T boundary.

Furthermore, methanogenesis and methanotrophy are believed to have influenced bulk δ¹³C_{org} in the zone 1. The extremely δ¹³C deficient methyl hopane compounds (−42 to −50‰) in the zone 1 confirmed the effect of methanotrophy [41,68]. So we should also consider the impact of recording burial of lacustrine methanotrophic biomass. Jones studied the chemical stratigraphy of Songliao Basin, found that OAE2 did not cause the increase of organic carbon burial in an expansive East Asian lake and attributed significant fluctuation in lacustrine δ¹³C_{org} to the global Bridgewick CIE and soil productivity in the Songliao catchment [28]. The sedimentary period of Kq1 occurred in the post evolution rift period of Songliao basin [11]. Therefor, the tectonic history of the Songliao Basin including episodes of thermal subsidence and sea transgression on the background of relatively passive tectonism and warm-wet climate with some residual greenhouse conditions after OAE2 could result in a unique combination of slow sedimentation in a moderately salted, stagnant lake and abundant vegetation in the surrounding land that may explain the anomalous records obtained in this study.

5. Conclusions

In this paper, the geochemical characteristics of oil shales and the influences of atmospheric CO₂ and seawater on the palaeoenvironment during formation of oil shale deposits were studied by using high-precision organic and inorganic geochemical data from detailed stratigraphic sampling of the Qingshankou Formation. The following conclusions were drawn:

- (1) The oil shales mainly occur in the zone one of the Qingshankou Formation. The oil shale thickness layer is 120 m, and the lithology is mainly grey-black and black shales. The sediments from the Qingshankou Formation in the Fuyu oilfield, possesses an excellent oil-generation potential.
- (2) Through changes in TOC, TS and TOC/TS ratio, the water environment during deposition of the Qingshankou Formation was a saline water environment with a high sulfate concentration. This water environment promoted an increased nutrient content and water density stratification in the lake basin. Oxygen consumption in the bottom water layer was conducive to the accumulation and burial of high-abundance of organic matter, forming the high-quality oil shales of the zone one of the Qingshankou Formation.
- (3) The oil shales are of high quality based on their high EOM (2.50–6.96 mg/g TOC) level and high yield of hydrocarbon fractions (48–89%).
- (4) The sources of the organic matter in the Qingshankou Formation oil shale are mainly zooplankton, algae and certain higher plants (including marine organisms), and the sedimentary environment of the Qingshankou Formation oil shale is a reductive saline water environment.

- (5) The global carbon cycle, warm-humid palaeoclimate, dynamic local biogeochemical cycling and relative passive tectonism were the most likely reasons for the TOC increase and negative $\delta^{13}\text{C}_{\text{org}}$ deviation.

Author Contributions: All authors contributed to the research in this paper. Y.S., W.G. and X.S. provided the data and funding. W.H. wrote the paper. S.S., S.Z., S.D., S.K. and X.Z. analyzed the data.

Funding: This work was supported by the National Nature Science Foundation of China (Grant No. 41790453), the Project of Jilin Province Development and Reform Commission of China, the Cooperative Project between Universities and Jilin Province, China (Grant No. SF2017-5-1), the Program for JLJU Science and Technology Innovative Research Team (Grant No. 2017TD-13), the Fundamental Research Funds for the Central Universities, and the self-determined Foundation of Key Laboratory of Oil Shale and Coexistent Energy Minerals of Jilin Province (Grant No. YYY-ZZ-18-03).

Conflicts of Interest: The authors declare no conflicts of interest.

References

1. Skelton, P.W.; Spicer, R.A.; Kelley, S.P.; Gilmour, I. *The Cretaceous World*; Cambridge University Press: London, UK, 2003.
2. Arthur, M.A.; Jenkyns, H.C.; Brumsack, H.J.; Schlanger, S.O. Stratigraphy, Geochemistry, and Paleoceanography of Organic Carbon-Rich Cretaceous Sequences. In *Cretaceous Resources Events, and Rhythms*; Ginsburg, R.N., Beaudoin, B., Eds.; Springer: New York, NY, USA, 1990; pp. 75–119.
3. Poulsen, C.J.; Barron, E.J.; Arthur, M.A.; Peterson, W.H. Response of the mid-Cretaceous global oceanic circulation to tectonic and CO₂ forcings. *Paleoceanography* **2001**, *16*, 576–592. [CrossRef]
4. Hong, S.K.; Lee, Y.I. Evaluation of atmospheric carbon dioxide concentrations during the Cretaceous. *Earth Planet. Sci. Lett.* **2012**, *327–328*, 23–28. [CrossRef]
5. Quan, C.; Sun, C.; Sun, Y. High resolution estimates of paleo-CO₂ Levels through the Campanian (Late Cretaceous) based on Ginkgo cuticles. *Cretac. Res.* **2009**, *30*, 424–428. [CrossRef]
6. Hou, D.; Feng, Z.; Huang, Q. Geological and Geochemical Evidences of Anoxic Event in The Songliao Basin, China. *Geoscience* **2003**, *17*, 311–317. (In Chinese)
7. Song, Z.G.; Qin, Y.; Geroge, S.C.; Wang, L.; Guo, J.T.; Feng, Z.H. A biomarker study of depositional paleoenvironments and source inputs for the massive formation of Upper Cretaceous lacustrine source rocks in the Songliao Basin, China. *Palaeogeogr. Palaeoclimatol. Palaeoecol.* **2013**, *385*, 137–151. [CrossRef]
8. Wan, X.Q.; Zhao, J.; Scott, R.W.; Wang, P.J.; Feng, Z.H.; Huang, Q.H.; Xi, D.P. Late Cretaceous stratigraphy, Songliao Basin, NE China: SK1 cores. *Palaeogeogr. Palaeoclimatol. Palaeoecol.* **2013**, *385*, 31–43. [CrossRef]
9. Wu, H.C.; Zhang, S.H. The floating astronomical time scale for the terrestrial Late Cretaceous Qingshankou Formation from the Songliao Basin of Northeast China and its stratigraphic and paleoclimate implications. *Earth Planet. Sci.* **2009**, *278*, 308–323. [CrossRef]
10. Khudololey, A.K.; Sokolov, S.D. Structural evolution of the northeast Asia continental margin: An example from the western Koryak fold and thrust belt (northeast Russia). *Geol. Mag.* **1998**, *135*, 311–330. [CrossRef]
11. Feng, Z.Q.; Jia, C.Z.; Xie, X.N.; Zhang, S.; Feng, Z.H.; Timothy, A.C. Tectonostratigraphic units and stratigraphic sequences of the nonmarine Songliao Basin, northeast China. *Basin Res.* **2010**, *22*, 79–95.
12. Wang, C.S.; Feng, Z.Q.; Zhang, L.M.; Huang, Y.J.; Cao, K.; Wang, P.J.; Zhao, B. Cretaceous paleogeography and paleoclimate and the setting of SK1 borehole sites in Songliao Basin, northeast China. *Palaeogeogr. Palaeoclimatol. Palaeoecol.* **2013**, *385*, 17–30. [CrossRef]
13. Liu, Z.; Sun, P.; Jia, J.; Liu, R.; Meng, Q. Distinguishing features and their genetic interpretation of stratigraphic sequences in continental deep water setting: A case from Qingshankou Formation in Songliao Basin. *Earth Sci. Front.* **2011**, *18*, 171–180. (In Chinese)
14. Liu, Z.; Wang, D.; Liu, L.; Liu, W.; Wang, P.; Du, X.; Yang, G. Sedimentary Characteristics of the Cretaceous Songliao Basin. *Acta Geol. Sin.* **1992**, *66*, 327–338.
15. Gao, R.; Kong, Q. Dinoflagellate and biomarker compounds of the Cretaceous non-marine source rocks in the Songliao Basin. *Discip. Dev. Res.* **1992**, *6*, 9–17. (In Chinese)
16. Hang, G.; Zhang, W.J. The Discussion of the Era of the Cretaceous Qingshankou Formation in Sngliao Basin. *Sci. Technol. Eng.* **2011**, *11*, 461–466.

17. Li, W.B. Palynoflora from the Quantou Formation of Songliao basin, NE China and its bearing on the Upper-Lower Cretaceous boundary. *Acta Palaeontol. Sin.* **2001**, *40*, 153–176. (In Chinese)
18. Wu, H.C.; Zhang, S.H. Establishment of floating astronomical time scale for the terrestrial Late Cretaceous Qingshankou Formation in the Songliao basin of Northeast China. *Earth Sci. Front.* **2008**, *15*, 159–169. [[CrossRef](#)]
19. Grock, D.R.; Hesselbo, S.P.; Jenkyns, H.C. Carbon isotope composition of lower cretaceous fossil wood: Ocean atmosphere chemistry and relation to sea level change. *Geology* **1999**, *27*, 155–158. [[CrossRef](#)]
20. Chen, P. Comments on the Classification and Correlation of Non-marine Jurassic and Cretaceous of China. *J. Stratigr.* **2000**, *24*, 114–119. (In Chinese)
21. Huang, Q.; Liu, J.; Xue, T.; Dang, Y.; Kong, H.; Zhang, W. Geochemical characteristics of anoxic event bed in Qingshankou Formation from the Well Chao 73–87 of Songliao Basin. *Chin. J. Geol.* **2009**, *44*, 435–443. (In Chinese)
22. Ye, D. The Significance of the Cretaceous Ostracoda Biostratigraphy and Magnetostratigraphy in Songliao Basin. *Pet. Geol. Oilfield Dev. Daqing* **1991**, *10*, 1–10. (In Chinese)
23. Ye, D.; Huang, Q.; Zhang, Y. *Ostracoda Biostratigraphy of the Cretaceous in Songliao Basin*; Petroleum Industry Press: Beijing, China, 2002.
24. Xi, D.; Wan, X.; Feng, Z.; Li, S.; Feng, Z.; Jia, J.; Jing, X.; Si, W. Discovery of Late Cretaceous foraminifera in the Songliao Basin: Evidence from SK-1 and implications for identifying seawater incursions. *Chin. Sci. Bull.* **2011**, *56*, 253–256. (In Chinese) [[CrossRef](#)]
25. Wang, Y. Preliminary study on the discovery and genesis of glauconite in the sediments of modern lakes in Fuxian Lake. *Chin. Sci. Bull.* **2013**, *2*, 14–17. (In Chinese)
26. Wang, M.; Lu, S.F.; Wang, Z.W.; Liu, Y.; Huang, W.B.; Chen, F.W.; Xu, X.Y.; Li, Z.; Li, J.J. Reservoir Characteristics of Lacustrine Shale and Marine Shale: Examples from the Songliao Basin, Bohai Bay Basin and Qiannan Depression. *Acta Geol. Sin.* **2016**, *90*, 1024–1038.
27. Wan, X.; Li, G.; Chen, P.; Yu, T.; Ye, D. Isotope Stratigraphy of the Cretaceous Qingshankou Formation in Songliao Basin and Its Correlation with Marine Cenomanian Stage. *Acta Geol. Sin.* **2005**, *79*, 150–156. (In Chinese)
28. Jones, M.M.; Ibarra, D.E.; Gao, Y.; Sageman, B.B.; Selby, D.; Chamberlain, C.P.; Graham, S.A. Evaluating Late Cretaceous OAEs and the influence of marine incursions on organic carbon burial in an expansive East Asian paleo-lake. *Earth Planet. Sci. Lett.* **2018**, *484*, 41–52. [[CrossRef](#)]
29. Peters, K.E.; Cassa, M.R. Applied source rock geochemistry. *Memoirs* **1994**, *60*, 93–120.
30. Espitalié, J.; Laporte, J.L.; Madec, M.; Marquis, F.; Leplat, P.; Pauletand, J.; Bouteleu, A. Methode rapide de caractérisation des roches meres, de leur potential petrolier et de leur degré d'évolution. *Rev. de l'Institut Fr. du Pet.* **1977**, *32*, 23–42.
31. Brunner, B.; Bernasconi, S.M.A. Revised isotope fractionation model for dissimilatory sulfate reduction in sulfate reducing bacteria. *Geochim. Cosmochim. Acta* **2005**, *69*, 4759–4771. [[CrossRef](#)]
32. Berner, R.A. Burial of organic carbon and pyrite sulfur in the modern ocean: Its geochemical and environmental significance. *Am. J. Sci.* **1982**, *282*, 451–475. [[CrossRef](#)]
33. Berner, R.A.; Raiswell, R. C/S method for distinguishing freshwater from marinesedimentary rocks. *Geology* **1984**, *12*, 365–368. [[CrossRef](#)]
34. Berner, R.A.; Raiswell, R. Burial of organic carbon and pyrite sulfur in sediments over Phanerozoic time: A new theory. *Geochim. Cosmochim. Acta* **1983**, *47*, 855–862. [[CrossRef](#)]
35. Leventhal, J.S. An interpretation of carbon and sulfur relationships in Black Sea sediments as indicators of environments of deposition. *Geochim. Cosmochim. Acta* **1983**, *47*, 133–138. [[CrossRef](#)]
36. Wilkin, R.T.; Arthur, M.A. Variations in pyrite texture, sulfur isotope composition, and iron systematics in the Black Sea: Evidence for Late Pleistocene to Holocene excursions of the O₂-H₂S redox transition. *Geochim. Cosmochim. Acta* **2001**, *65*, 1399–1416. [[CrossRef](#)]
37. Sachse, V.F.; Littke, R.; Jabour, H.; Schühmann, T.; Kluth, O. Late Cretaceous (Late Turonian, Coniacian and Santonian) petroleum source rocks as part of an OAE, Tarfaya Basin, Morocco. *Mar. Pet. Geol.* **2012**, *29*, 35–49. [[CrossRef](#)]
38. Prauss, M.L. Marine palynology of the Oceanic Anoxic Event 3 (OAE3, Coniacian–Santonian) at Tarfaya, Morocco, NW Africa. The transition from preservation to production controlled accumulation of marine organic carbon. *Cretac. Res.* **2015**, *53*, 19–37. [[CrossRef](#)]

39. Dean, W.E.; Gorham, E. Magnitude and significance of carbon burial in lakes, reservoirs, and peatlands. *Geology* **1998**, *26*, 535–538. [CrossRef]
40. Jia, J.; Bechtel, A.; Liu, Z.; Strobl, S.A.I.; Sun, P.; Sachsenhofer, R.F. Oil shale formation in the Upper Cretaceous Nenjiang Formation of the Songliao Basin (NE China): Implications from organic and inorganic geochemical analyses. *Int. J. Coal Geol.* **2013**, *113*, 11–26. [CrossRef]
41. Bechtel, A.; Jia, J.; Strobl, S.A.I.; Sachsenhofer, R.F.; Liu, Z.; Gratzer, R.; Püttmann, W. Palaeoenvironmental conditions during deposition of the Upper Cretaceous oilshale sequences in the Songliao Basin (NE China): Implications from geochemical analysis. *Org. Geochem.* **2012**, *46*, 76–95. [CrossRef]
42. Song, Y.; Liu, Z.; Meng, Q.; Xu, J. The Geochemical Characteristics and Its Implication of Organic Matter Enrichment Conditions in the Upper Cretaceous Oil Shale Sequences of the Songliao Basin (NE China). *Acta Geol. Sin.* **2015**, *89*, 268–269. (In Chinese) [CrossRef]
43. Liang, Y.; Shan, X.; Yousif, M.; Makeen, W.H.A.; Hao, G.; Tong, L.; Mutari, L.; Zhao, R.; Habeeb, A. Ayinla, Geochemical Characteristics of Oil from Oligocene Lower Ganchaigou Formation Oil Sand in Northern Qaidam Basin, China. *Nat. Resour. Res.* **2019**, *28*, 1521–1546. [CrossRef]
44. Collister, J.W.; Lichtfouse, E.; Hieshima, G.; Hayes, J.M. Partial resolution of sources of n-alkanes in the saline portion of the Parachute Creek Member, Green River Formation. *Org. Geochem.* **1994**, *21*, 645–659. [CrossRef]
45. Lijmbach, G.W. SP (1) On the Origin of Petroleum. In Proceedings of the 9th World Petroleum Congress, Tokyo, Japan, 11–16 May 1975.
46. Volkman, J.K.; Maxwell, J.R. Acyclic isoprenoids as biological markers. In *Biological Markers in the Sedimentary Record*; Johns, R.B., Ed.; Elsevier: Amsterdam, The Netherlands, 1986.
47. Shanmugam, G. Significance of coniferous rainforests and related organic matter in generating commercial quantities of oil, Gipps-land Basin, Australia. *AAPG Bull.* **1985**, *69*, 1241–1254.
48. Makeen, Y.M.; Abdullah, W.H.; Hakimi, M.H. Biological markers and organic petrology study of organic matter in the Lower Cretaceous Abu Gabra sediments (Muglad Basin, Sudan): Origin, type and palaeoenvironmental conditions. *Arab. J. Geosci.* **2015**, *8*, 489–506. [CrossRef]
49. Makeen, Y.M.; Abdullah, W.H.; Hakimi, M.H. The origin, type and preservation of organic matter of the Barremian Aptian organic-rich shales in the Muglad Basin, Southern Sudan, and their relation to paleoenvironmental and paleoclimate conditions. *Mar. Pet. Geol.* **2015**, *65*, 187–197. [CrossRef]
50. Makeen, Y.M.; Abdullah, W.H.; Hakimi, M.H.; Elhassan, O.M.A. Organic geochemical characteristics of the lower Cretaceous Abu Gabra formation in the great Moga oilfield, Muglad Basin, Sudan: Implications for depositional environment and oil-generation potential. *J. Afr. Earth Sci.* **2015**, *103*, 102–112. [CrossRef]
51. Qin, J.; Wang, S.; Sanei, H.; Jiang, C.; Chen, Z.; Ren, S.; Xu, X.; Yang, J.; Zhong, N. Revelation of organic matter sources and sedimentary environment characteristics for shale gas formation by petrographic analysis of middle Jurassic Dameigou formation, northern Qaidam Basin, China. *Int. J. Coal Geol.* **2018**, *195*, 373–385. [CrossRef]
52. Huang, W.Y.; Meinschein, W.G. Sterols as ecological indicators. *Geochim. Cosmochim. Acta* **1979**, *43*, 739–745. [CrossRef]
53. Peters, K.E.; Moldowan, J.M. The biomarker guide: Interpreting molecular fossils in petroleum and ancient sediments. *Choice Rev. Online* **1993**, *30*, 30–2690.
54. Mello, M.R.; Telnaes, N.; Gaglianone, P.C.; Chicarelli, M.I.; Brassell, S.C.; Maxwell, J.R. Organic geochemical characterization of depositional palaeoenvironments of source rocks and oils in Brazilian marginal basins. *Org. Geochem.* **1988**, *13*, 31–45. [CrossRef]
55. Sofer, Z.V. Isotopic composition of individual n-alkane in oils. *Org. Geochem.* **1992**, *23*, 210–212.
56. Zhao, M.; Huang, D. Carbon Isotopic Distributive Characteristics of Crude Oil Monomers Produced in Different Sedimentary. *Environ. Pet. Geol.* **1995**, *17*, 171–179.
57. Schlanger, S.O.; Arthur, M.A. The Cenomanian-Turonian oceanic anoxic event, 1. Stratigraphy and distribution of organic carbon-rich beds and the marine excursion. *Geol. Soc.* **1987**, *26*, 371–399.
58. Sageman, B.B.; Meyers, S.R.; Arthur, M.A. Orbital time scale and new C-isotope record for Cenomanian-Turonian boundary stratotype. *Geology* **2006**, *34*, 125–128. [CrossRef]
59. Barclay, R.S.; McElwain, J.C.; Sageman, B.B. Carbon sequestration activated by a volcanic CO₂ pulse during Ocean Anoxic Event 2. *Nat. Geosci.* **2010**, *3*, 205–208. [CrossRef]

60. Hong, S.K.; Lee, Y.I. Contributions of soot to $\delta^{13}\text{C}$ of organic matter in Cretaceous lacustrine deposits, Gyeongsang Basin, Korea: Implication for paleoenvironmental reconstructions Santonian-Campanian Boundary Event. *Palaeogeogr. Palaeoclimatol. Palaeoecol.* **2013**, *371*, 54–61. [[CrossRef](#)]
61. Pucéat, E.; Lécuyer, C.; Sheppard, S.M.F.; Dromart, G.; Reboulet, S.; Grandjean, P. Thermal evolution of Cretaceous Tethyan marine waters inferred from oxygen isotope composition of fish tooth enamels. *Paleoceanography* **2003**, *18*, 1–7. [[CrossRef](#)]
62. Wilson, P.A.; Norris, R.D.; Cooper, M.J. Testing the Cretaceous greenhouse hypothesis using glassy foraminiferal calcite from the core of the Turonian tropics on Demerara Rise. *Geology* **2002**, *30*, 607–610. [[CrossRef](#)]
63. Erba, E. Calcareousnannofossils and Mesozoic oceanic anoxic events. *Mar. Micropaleontol.* **2004**, *52*, 85–106. [[CrossRef](#)]
64. Jones, C.E.; Jenkyns, H.C. Sea water strontium isotopes oceanic anoxic events and sea floor hydro thermal activity in the Jurassic and Cretaceous. *Am. J. Sci.* **2001**, *301*, 112–149. [[CrossRef](#)]
65. Sinton, C.; Duncan, R. Potential links between ocean plate auvolcanism and global ocean anoxia at the Cenomanian-Turonian boundary. *Econ. Geol.* **1999**, *92*, 836–842. [[CrossRef](#)]
66. Diefendorf, A.F.; Mueller, K.E.; Wing, S.L.; Freeman, K.H. Global patterns in leaf $\delta^{13}\text{C}$ discrimination and implications for studies of past and future climate. *PNAS* **2009**, *107*, 5738–5743. [[CrossRef](#)] [[PubMed](#)]
67. Yan, J. Mid-Cretaceous Biostratigraphy and Palaeoclimate Change from the Qingshankou and Nenjiang Formations in Nong'an area, Jijin Province. Master's Thesis, China University of Geosciences, Beijing, China, 2009.
68. Hollander, D.J.; Smith, M.A. Microbially mediated carbon cycling as a control on the delta C-13 of sedimentary carbon in eutrophic lake mendota (USA): New models for interpreting isotopic excursions in the sedimentary record. *Geochim. Cosmochim. Acta* **2001**, *65*, 4321–4337. [[CrossRef](#)]



© 2019 by the authors. Licensee MDPI, Basel, Switzerland. This article is an open access article distributed under the terms and conditions of the Creative Commons Attribution (CC BY) license (<http://creativecommons.org/licenses/by/4.0/>).